

Anomalous dependence of the c -axis polarized Fe B_{1g} phonon mode with Fe and Se concentrations in $\text{Fe}_{1+y}\text{Te}_{1-x}\text{Se}_x$

Y.J. Um,¹ A. Subedi,¹ P. Toulemonde,² A.Y. Ganin,³ L. Boeri,¹ M. Rahlenbeck,¹ Y. Liu,¹ C.T. Lin,¹ S.J.E. Carlsson,² A. Sulpice,^{2,4} M.J. Rosseinsky,³ B. Keimer,¹ and M. Le Tacon¹

¹Max-Planck-Institut für Festkörperforschung, Heisenbergstrasse 1, D-70569 Stuttgart, Deutschland

²Institut Néel, CNRS & UJF, 25 avenue des martyrs, F-38042 Grenoble cedex 09, France

³Department of Chemistry, University of Liverpool, Liverpool, L69 7ZD, United Kingdom

⁴CRETA, CNRS & UJF, 25 avenue des martyrs, F-38042 Grenoble cedex 09, France

(Dated: December 6, 2018)

We report on an investigation of the lattice dynamical properties in a range of $\text{Fe}_{1+y}\text{Te}_{1-x}\text{Se}_x$ compounds, with special emphasis on the c -axis polarized vibration of Fe with B_{1g} symmetry, a Raman active mode common to all families of Fe-based superconductors. We have carried out a systematic study of the temperature dependence of this phonon mode as a function of Se x and excess Fe y concentrations. In parent compound Fe_{1+y}Te , we observe an unconventional broadening of the phonon between room temperature and magnetic ordering temperature T_N . The situation smoothly evolves toward a regular anharmonic behavior as Te is substituted for Se and long range magnetic order is replaced by superconductivity. Irrespective to Se contents, excess Fe is shown to provide an additional damping channel for the B_{1g} phonon at low temperatures. We performed Density Functional Theory *ab initio* calculations within the local density approximation to calculate the phonon frequencies including magnetic polarization and Fe non-stoichiometry in the virtual crystal approximation. We obtained a good agreement with the measured phonon frequencies in the Fe-deficient samples, while the effects of Fe excess are poorly reproduced. This may be due to excess Fe-induced local magnetism and low energy magnetic fluctuations that can not be treated accurately within these approaches. As recently revealed by neutron scattering and muon spin rotation studies, these phenomena occur in the temperature range where anomalous decay of the B_{1g} phonon is observed and suggests a peculiar coupling of this mode with local moments and spin fluctuations in $\text{Fe}_{1+y}\text{Te}_{1-x}\text{Se}_x$.

PACS numbers: 74.70.Xa, 74.25.nd, 74.25.Kc

I. INTRODUCTION

The recent discovery of superconductivity in F-doped LaFeAsO with T_c of ~ 26 K created a flurry of excitement in condensed matter research.¹ Rapidly, numerous families of Fe-based superconductors such as $RE\text{FeAs}(\text{O}_{1-x}\text{F}_x)$ (1111-family, $RE = \text{rare earth}$), $M\text{Fe}_2\text{As}_2$ (122-family, $M = \text{Ba, Ca, Sr, K, Cs ...}$), $\text{LiFeAs}/\text{NaFeAs}$ (111-family) and $\text{Fe}_{1+y}\text{Te}_{1-x}\text{Se}_x$ (11-family)²⁻⁸ have been found and investigated. Although the $\text{Fe}_{1+y}\text{Te}_{1-x}\text{Se}_x$ chalcogenides share with their pnictogen-based cousins similar structure, based on planar layers of edge sharing $[\text{Fe}(\text{Se,Te})_4]$ tetrahedra, some significant differences were rapidly revealed. Among them are the large magnetic moment ($\sim 2.0\text{-}2.5 \mu_B$) and the double stripe magnetic ordering of the parent Fe_{1+y}Te compound.^{9,10} Magnetic stripes are found in other Fe-based parent compounds such as BaFe_2As_2 or LaFeAsO stripes in pnictides, but they are rotated by 45° around the c -axis with respect to Fe_{1+y}Te ,¹⁰⁻¹³ with significantly lower magnetic moments on Fe in these compound (typically $0.4\text{-}1.0 \mu_B/\text{iron}$ ^{14,15}).

The magnetic ordering is accompanied by a structural transition ($T_N \sim 67\text{K}$),⁹ which can be progressively suppressed on substitution of isovalent Se at the Te 2b Wyckoff position. This also results in emergence of superconductivity with a $T_c^{\text{max}} \sim 14$ K at ambient pressure at the

optimum doping.^{6,7} However, numerous reports have recently demonstrated that the excess of interstitial Fe between the chalcogenide layers, even after doping with Se, could affect both superconducting and magnetic properties, *e.g.* suppression of transition temperature T_c or lowering shielding fraction, as well as leading to the appearance of weakly localized magnetic states.¹⁶⁻²²

Raman spectroscopy is an ultimate noninvasive tool and can allow systematic studies of the temperature dependence of the phonon spectrum as function of Se and excess of interstitial Fe. For example, Raman spectroscopy has proved useful in the understanding of the structural, magnetic and electronic properties of superconducting pnictides.²³⁻³⁶ Available Raman data on single crystals of $\text{Fe}_{1+y}\text{Te}_{1-x}\text{Se}_x$ is to date limited. In refs. 37 and 38, comparison between Se-substituted and parent Fe_{1+y}Te samples is made, but neither temperature dependence nor influence of the excess iron concentration on the lattice dynamics are discussed. In ref. 39, the authors study the evolution with temperature of the Raman spectra of $\text{Fe}_{1.05}\text{Te}$, with a particular emphasis on the anomalously large lineshape of the Te A_{1g} phonon. It is argued to originate from a peculiar spin-orbital frustration effect, that leaves unaffected the B_{1g} phonon after symmetry considerations.

In this paper, we focus mainly on this Raman active c -axis polarized optical phonon in $\text{Fe}_{1+y}\text{Te}_{1-x}\text{Se}_x$, which

is common to all the iron-based superconductors families, and discuss its evolution with temperature for various Fe, y , and Se content, x . We can demonstrate that contrarily to the A_{1g} mode, the observed temperature dependence is strongly affected by composition. To some extent, the phonon behavior through the various phases transitions (depending of the Se content) is consistent with those of the c -axis polarized Fe modes reported in the other families of Fe-based superconductors (*e.g.* 122 and 111). The narrowing of the phonon lineshape through the magnetic transition of the parent compound or the absence of renormalization through the superconducting one are for instance reported. On the other hand, we also show that in some specific conditions, the behavior of the B_{1g} mode seriously deviates from the aforementioned one. The phonon linewidth shows an anomalous broadening in the paramagnetic state of Fe_{1+y}Te parent compounds and an unusually strong dependence with the Se concentration in the doped compounds. Further anomalies, indicative of additional decay channels, are found when increasing the concentration of excess Fe y .

To try to get some insights about the influence of excess iron on the Raman phonon, we have carried out a Density Functional Theory (DFT) *ab initio* calculation within the local density approximation (LDA) of the phonon frequencies, including the effects of magnetism and Fe nonstoichiometry in the virtual crystal approximation (VCA). The measured frequencies are in good agreement with the predicted ones, including a softening with increasing Fe content in Fe deficient samples, but the effects of Fe nonstoichiometry are poorly reproduced.

Recent studies of magnetic properties have revealed that excess Fe induces local magnetism and low energy magnetic fluctuations,^{21,40} but these can not be treated within our DFT approaches. Generally speaking, whenever low-energy magnetic fluctuations are at play, the B_{1g} phonon behavior deviates from the conventional harmonic picture and cannot be reproduced within our theoretical framework. This suggests that the reported anomalies originate from coupling between the B_{1g} mode and these excitations.

II. EXPERIMENTAL DETAILS

In order to discriminate the effects of Fe excess and of Se substitution, we have studied different groups of crystals, listed in Table I. In the first group, no Se was present and only the Fe concentration was changed Fe_{1+y}Te ($\text{Fe}_{1.02}\text{Te}$, $\text{Fe}_{1.09}\text{Te}$). In the second group we changed the Se concentration while keeping the Fe concentration as close from 1 as possible ($\text{Fe}_{1.00}\text{Te}_{0.78}\text{Se}_{0.22}$, $\text{Fe}_{0.99}\text{Te}_{0.69}\text{Se}_{0.31}$, $\text{Fe}_{0.98}\text{Te}_{0.66}\text{Se}_{0.34}$ and $\text{Fe}_{0.95}\text{Te}_{0.56}\text{Se}_{0.44}$). Finally, we also studied Se-substituted samples containing sizable excess iron ($\text{Fe}_{1.05}\text{Te}_{0.58}\text{Se}_{0.42}$, $\text{Fe}_{1.08}\text{Te}_{0.73}\text{Se}_{0.27}$). $\text{Fe}_{1+y}\text{Te}_{1-x}\text{Se}_x$ single crystals were grown in sealed quartz tube as described elsewhere^{41–44}. The chemical compositions listed

TABLE I: A summary of the chemical compositions obtained by EDX and characteristic transition temperatures of the various $\text{Fe}_{1+y}\text{Te}_{1-x}\text{Se}_x$ samples used in this study.

Sample Composition	T_N	T_c
$\text{Fe}_{1.02}\text{Te}$	67 K	—
$\text{Fe}_{1.09}\text{Te}$	65 K	—
$\text{Fe}_{1.00}\text{Te}_{0.78}\text{Se}_{0.22}$	—	11.5 K
$\text{Fe}_{0.99}\text{Te}_{0.69}\text{Se}_{0.31}$	—	11 K
$\text{Fe}_{0.98}\text{Te}_{0.66}\text{Se}_{0.34}$	—	10.5 K
$\text{Fe}_{0.95}\text{Te}_{0.56}\text{Se}_{0.44}$	—	14 K
$\text{Fe}_{1.05}\text{Te}_{0.58}\text{Se}_{0.42}$	—	11.5 K
$\text{Fe}_{1.08}\text{Te}_{0.73}\text{Se}_{0.27}$	—	9 K

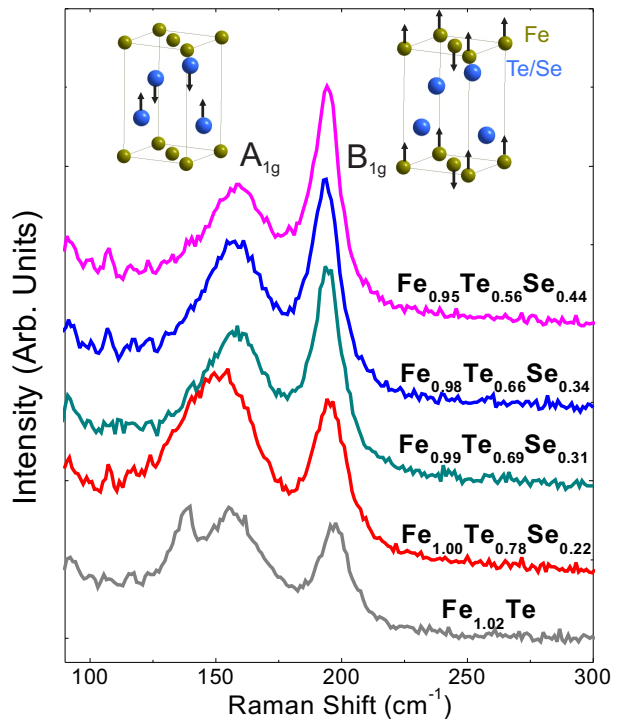


FIG. 1: (Color online) Room temperature Raman spectra of the $\text{Fe}_{1.02}\text{Te}$, $\text{Fe}_{1.00}\text{Te}_{0.78}\text{Se}_{0.22}$, $\text{Fe}_{0.99}\text{Te}_{0.69}\text{Se}_{0.31}$, $\text{Fe}_{0.98}\text{Te}_{0.66}\text{Se}_{0.34}$, and $\text{Fe}_{0.95}\text{Te}_{0.56}\text{Se}_{0.44}$ samples (see Table I). Spectra have been shifted vertically for clarity. Eigendisplacements corresponding to the $A_{1g}(\text{Te/Se})$ and $B_{1g}(\text{Fe})$ are represented schematically.

in Table I were determined using energy dispersive x-ray spectroscopy (EDX), and the antiferromagnetic (AF) and superconducting (SC) transition temperatures T_N and T_c were measured by use of a superconducting quantum interference device magnetometer.

All Raman light scattering experiments were performed on freshly cleaved surface of $\text{Fe}_{1+y}\text{Te}_{1-x}\text{Se}_x$ single crystals. All the samples were mounted in a helium-flow cryostat allowing measurements between 5 K and room temperature. Spectra were taken in backscattering ge-

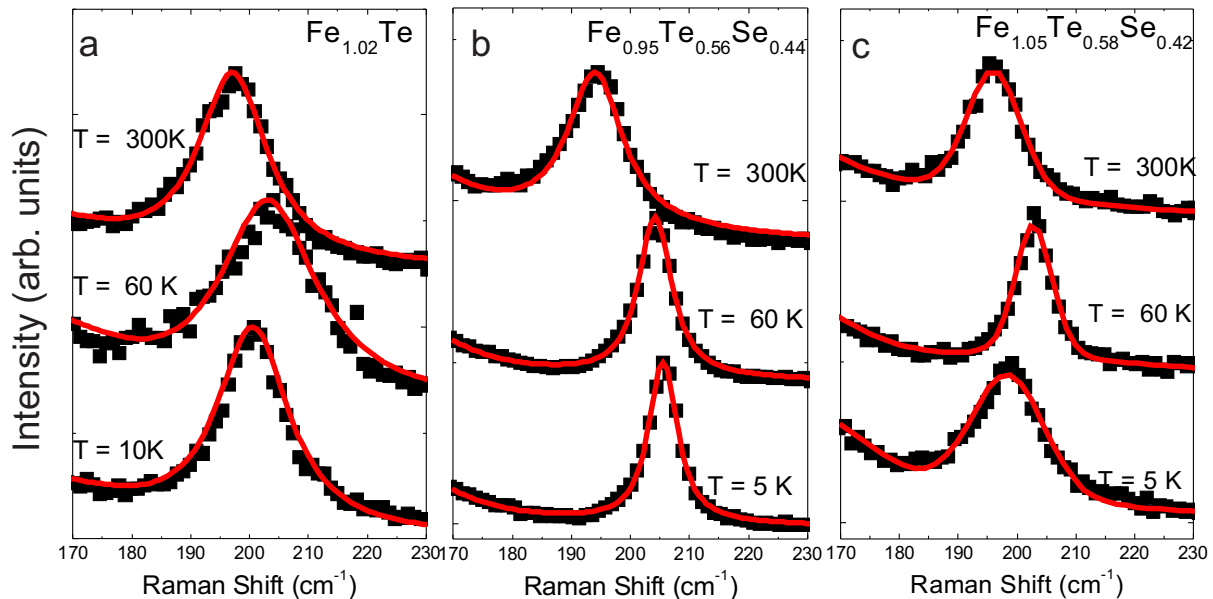


FIG. 2: (Color online) a) B_{1g} phonon of the $\text{Fe}_{1.02}\text{Te}$ sample for selected temperatures (room temperature, $T \sim T_N$ and base temperature). Black squares are the data, and the red line is the fit following the procedure described in the text. Phonon intensity have been normalized and the spectra have been shifted vertically for clarity. b) Same plot for the $\text{Fe}_{0.95}\text{Te}_{0.56}\text{Se}_{0.44}$ sample. c) same plot for the $\text{Fe}_{1.05}\text{Te}_{0.58}\text{Se}_{0.42}$ sample.

ometry through a JobinYvon LabRam 1800 single grating spectrometer equipped with a razor-edge filter and a Peltier-cooled charge-coupled-device camera. We used a linearly polarized He^+/Ne^+ mixed gas laser with $\lambda = 632.817$ nm for excitation. The laser beam was focused through a $50\times$ microscope objective to ~ 5 μm diameter spot on the sample surface. The power of the incident laser was kept less than 1 mW to avoid laser-induced heating. In order to determine the precise frequency of phonons for each temperature, Neon emission lines were recorded between each measurements. For data analysis, all phonon peaks were fitted by Lorentzian profiles, convoluted with the spectrometer resolution function (a Gaussian line of 2 cm^{-1} full width at half maximum (FWHM)).

III. EXPERIMENTAL RESULTS

A. Influence of Se doping

In Fig. 1 we show the Raman spectrum measured at room temperature on the Se-free $\text{Fe}_{1.02}\text{Te}$ sample, together with the $\text{Fe}_{1.00}\text{Te}_{0.78}\text{Se}_{0.22}$, $\text{Fe}_{0.99}\text{Te}_{0.69}\text{Se}_{0.31}$, $\text{Fe}_{0.98}\text{Te}_{0.66}\text{Se}_{0.34}$ and $\text{Fe}_{0.95}\text{Te}_{0.56}\text{Se}_{0.44}$ superconducting samples that all have a Fe stoichiometry close to 1. From symmetry consideration, one expects four Raman active modes: $A_{1g}(\text{Te/Se})$, $B_{1g}(\text{Fe})$, $E_g(\text{Te})$, $E_g(\text{Fe})$. Raman measurement have been performed in backscattering geometry, with the incident light polarization along the a -axis of the single crystal. An analyzer has been used to check the phonon selection rules, but most of the measurements presented here have been performed without in order to maximize the phonon peak intensities.

In this scattering geometry, only the $A_{1g}(\text{Te/Se})$ and $B_{1g}(\text{Fe})$ modes, sketched in Fig. 1, are present. As seen in Fig. 1, these modes are found at ~ 155 cm^{-1} and ~ 197

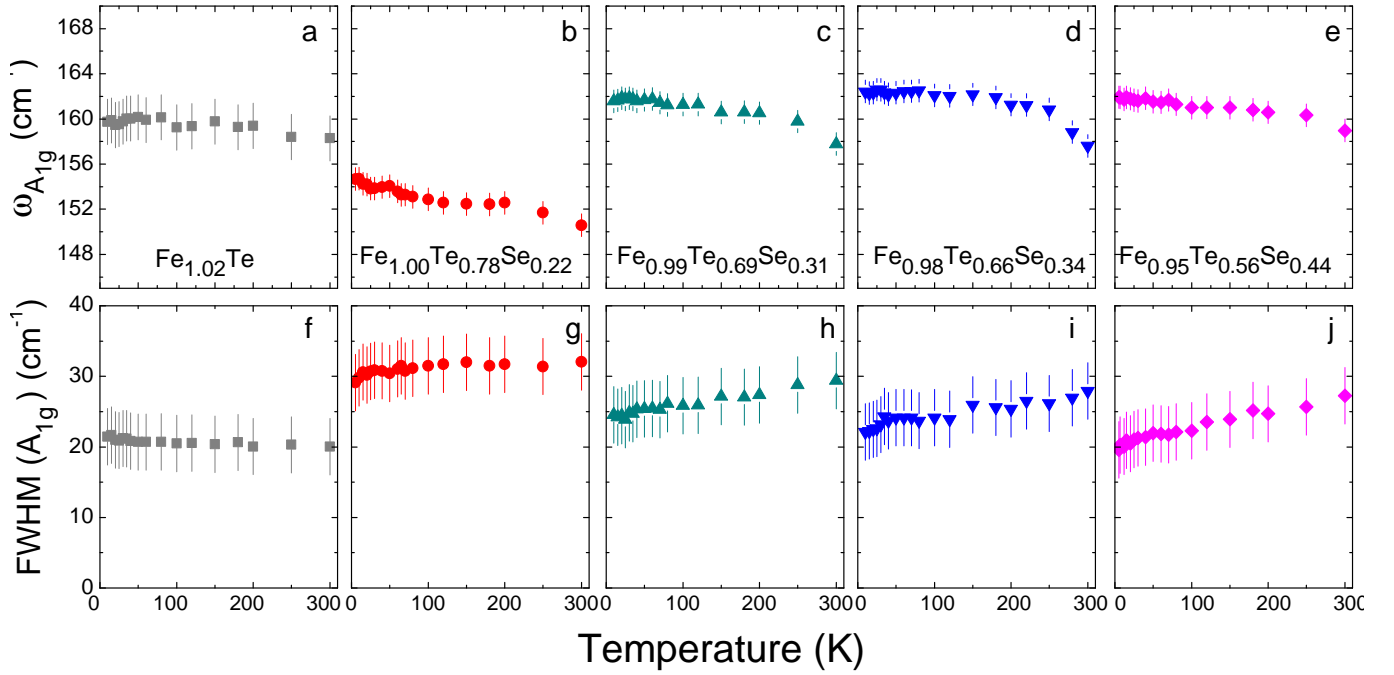


FIG. 3: (Color online) Upper panel: Temperature dependence of the A_{1g} (Te/Se) mode frequency of the a) Fe_{1.02}Te, b) Fe_{1.00}Te_{0.78}Se_{0.22}, c) Fe_{0.99}Te_{0.69}Se_{0.31}, d) Fe_{0.98}Te_{0.66}Se_{0.34}, and e) Fe_{0.95}Te_{0.56}Se_{0.44} samples. Lower panel: Temperature dependence of the A_{1g} (Te/Se) mode FWHM of the f) Fe_{1.02}Te, g) Fe_{1.00}Te_{0.78}Se_{0.22}, h) Fe_{0.99}Te_{0.69}Se_{0.31}, i) Fe_{0.98}Te_{0.66}Se_{0.34}, and j) Fe_{0.95}Te_{0.56}Se_{0.44} samples.

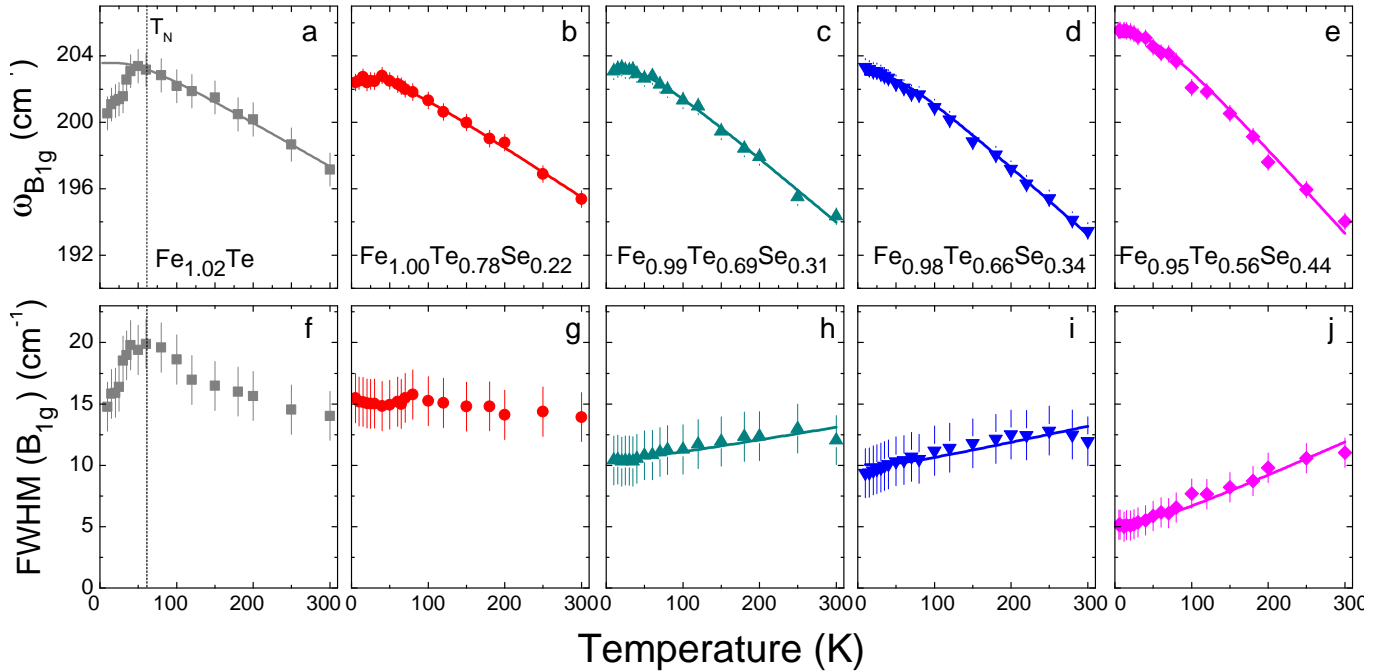


FIG. 4: (Color online) Upper panel: Temperature dependence of the B_{1g} (Fe) mode frequency of the a) Fe_{1.02}Te, b) Fe_{1.00}Te_{0.78}Se_{0.22}, c) Fe_{0.99}Te_{0.69}Se_{0.31}, d) Fe_{0.98}Te_{0.66}Se_{0.34}, and e) Fe_{0.95}Te_{0.56}Se_{0.44} samples. Lower panel: Temperature dependence of the B_{1g} (Fe) mode full-width-half-maximum of the f) Fe_{1.02}Te, g) Fe_{1.00}Te_{0.78}Se_{0.22}, h) Fe_{0.99}Te_{0.69}Se_{0.31}, i) Fe_{0.98}Te_{0.66}Se_{0.34}, and j) Fe_{0.95}Te_{0.56}Se_{0.44} samples. Solid lines are fits of the temperature dependence of the B_{1g} phonon frequency and linewidth in the various samples using the anharmonic model described in the text.

cm^{-1} at room temperature, respectively, in agreement with previous reports^{37–39}. These two peaks are much broader than in any of the other iron pnictides^{25–27}. The large A_{1g} mode linewidth ($\sim 20 \text{ cm}^{-1}$ at room temperature in $\text{Fe}_{1.02}\text{Te}$, almost 3 times larger than the A_{1g} As mode in BaFe_2As_2 ²⁵) has been attributed to spin-orbital frustration effects.³⁹ In the parent $\text{Fe}_{1.02}\text{Te}$ single crystal, an additional peak was observed around 136 cm^{-1} . The origin of this mode remains unclear. It is temperature independent (and cannot, therefore, be attributed to the lowering of the crystal symmetry induced by the structural transition), and has been observed irrespective of the Fe excess concentration (see Fig. 5-a). It is not observed in the Se-rich compounds (see Fig. 1). In contrast with the results of Xia *et al.* in ref. 37, claiming the disappearance of the A_{1g} mode in the Raman spectra of $\text{FeTe}_{0.92}$ and $\text{Fe}_{1.03}\text{Te}_{0.7}\text{Se}_{0.3}$ with increasing Se concentration, the mode is clearly visible in all the investigated compounds.

The frequency of the two phonons is weakly dependent on Se contents: at the lowest recorded temperatures (5 K) it remains essentially constant for Se contents between 22% and 34% ($\text{Fe}_{1.00}\text{Te}_{0.78}\text{Se}_{0.22}$ and $\text{Fe}_{0.98}\text{Te}_{0.66}\text{Se}_{0.34}$), while a small hardening ($\sim 2 \text{ cm}^{-1}$) is observed for the sample with 44% of Se ($\text{Fe}_{0.95}\text{Te}_{0.56}\text{Se}_{0.44}$). This latter effect may be caused by the significant Fe deficiency in the $\text{Fe}_{0.95}\text{Te}_{0.56}\text{Se}_{0.44}$ sample (see Secs. IV and V B 2). Within our experimental errors, this seems to be also the case for the A_{1g} phonon, as trivially expected from the substitution of Te with lighter Se (the mode frequency going, in first approximation, as $M^{-1/2}$, with M denoting the reduced mass of the considered oscillator). The only noticeable exception, is the $\text{Fe}_{1.00}\text{Te}_{0.78}\text{Se}_{0.22}$ sample, where the A_{1g} mode is broader and softer than in any other compounds. This may originate from an overlapping of the A_{1g} mode with the 136 cm^{-1} peak observed in the parent compounds. It seems that for this particular doping level the modes energies are still separated enough to cause an apparent broadening and shift to lower frequency of the total envelope, but not enough to allow to resolve them individually.

In Figs. 2-a and -b, we show details of the fitting for the $\text{Fe}_{1.02}\text{Te}$ and $\text{Fe}_{0.95}\text{Te}_{0.56}\text{Se}_{0.44}$ samples, that illustrates one of the main findings of our study, *i.e.* the strong changes in the temperature dependence of the B_{1g} phonon on doping. In the undoped $\text{Fe}_{1.02}\text{Te}$ sample, the B_{1g} mode hardens and broadens with decreasing temperature down to T_N , and then softens and narrows down to base temperature. For the $\text{Fe}_{0.95}\text{Te}_{0.56}\text{Se}_{0.44}$ sample with the highest Se concentration, we observed a continuous hardening and narrowing of the mode the whole way down to 5 K. In Figs. 3 and 4, respectively, we report the full temperature dependence of the frequency of the two c -axis polarized modes for the five samples with Fe concentration close to 1. The temperature dependencies of the linewidths for the same samples are given in the lower panels of these figures.

While the temperature is decreased, a hardening of

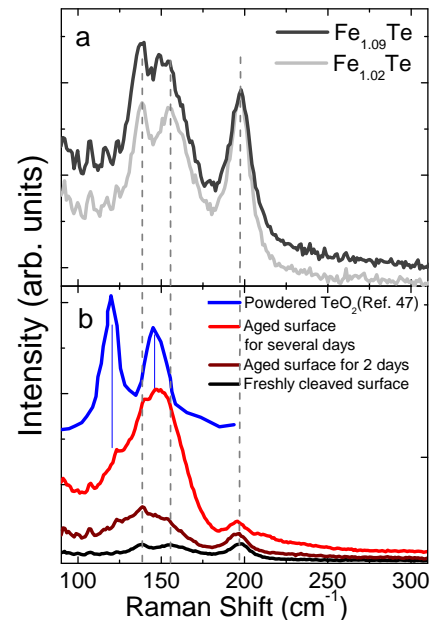


FIG. 5: (Color online) a) Room temperature Raman spectra of the parent $\text{Fe}_{1.02}\text{Te}$ and $\text{Fe}_{1.09}\text{Te}$ samples (vertically shifted for clarity). b) Example of the aging effect on the parent single crystals. The spectrum of powdered TeO_2 from ref.⁴⁷ has been added for comparison.

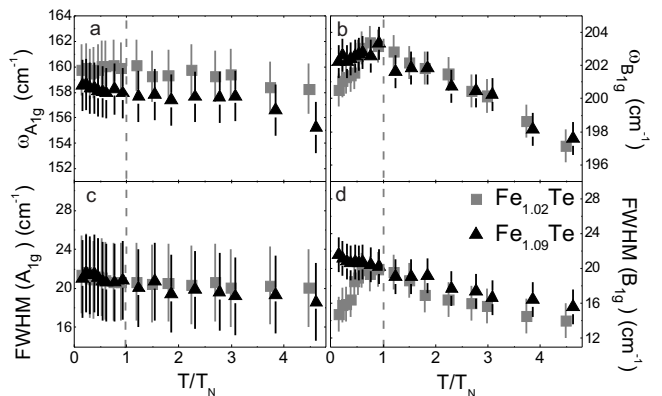


FIG. 6: (Color online) a) and b) Temperature dependence of the frequency the A_{1g} and B_{1g} modes in these samples. c) and d) Temperature dependence of the linewidth the A_{1g} and B_{1g} modes in these samples.

both the A_{1g} and B_{1g} modes in all the systems is observed, as expected from the lattice contraction. No noticeable differences between the samples are seen. As we go through the magnetic transition in the $\text{Fe}_{1.02}\text{Te}$ parent compound, a clear softening of the B_{1g} mode is observed (see also Fig. 6), while no changes across T_c occur in the samples containing Se. Within our error bars, the A_{1g} mode frequency remains essentially unaffected by these transitions. As shown in Fig. 3 weak narrowing of the A_{1g} line with decreasing tempera-

TABLE II: Fitting parameters for the temperature dependence of the B_{1g} phonon linewidth in $\text{Fe}_{0.99}\text{Te}_{0.69}\text{Se}_{0.31}$, $\text{Fe}_{0.98}\text{Te}_{0.66}\text{Se}_{0.34}$ and $\text{Fe}_{0.95}\text{Te}_{0.56}\text{Se}_{0.44}$ samples.

Sample	ω_0 (cm^{-1})	Γ_0 (cm^{-1})	Γ (cm^{-1})
$\text{Fe}_{0.99}\text{Te}_{0.69}\text{Se}_{0.31}$	203.9	9.9	0.78
$\text{Fe}_{0.98}\text{Te}_{0.66}\text{Se}_{0.34}$	203.8	9.8	0.78
$\text{Fe}_{0.95}\text{Te}_{0.56}\text{Se}_{0.44}$	205.6	3.44	2.1

ture is observed for $\text{Fe}_{0.99}\text{Te}_{0.69}\text{Se}_{0.31}$, $\text{Fe}_{0.98}\text{Te}_{0.66}\text{Se}_{0.34}$ and $\text{Fe}_{0.95}\text{Te}_{0.56}\text{Se}_{0.44}$ samples, while its broad linewidth remains essentially temperature independent in the $\text{Fe}_{1.02}\text{Te}$ and $\text{Fe}_{1.00}\text{Te}_{0.78}\text{Se}_{0.22}$ sample. In parallel to this, an unusual evolution on Se doping of the temperature dependence of the B_{1g} mode linewidth can be seen in the lower panels of Fig. 4. Starting from the almost half-doped $\text{Fe}_{0.95}\text{Te}_{0.56}\text{Se}_{0.44}$ compound, a conventional behavior is observed: as in most of the materials, this mode narrows with decreasing temperature (the phonon width is inversely proportional to its lifetime, which is expected to increase as the phonon-phonon interaction is reduced when decreasing the temperature^{45,46}). Decreasing Se concentration toward the parent $\text{Fe}_{1.02}\text{Te}$ sample, a smooth evolution from this regular behavior is observed: in $\text{Fe}_{0.99}\text{Te}_{0.69}\text{Se}_{0.31}$ and $\text{Fe}_{0.98}\text{Te}_{0.66}\text{Se}_{0.34}$ samples only a weak narrowing of the phonon is observed between room and base temperature, while in $\text{Fe}_{1.00}\text{Te}_{0.78}\text{Se}_{0.22}$ and $\text{Fe}_{1.02}\text{Te}$ the phonon essentially broadens as temperature is decreased. Below the magnetic ordering transition in the $\text{Fe}_{1.02}\text{Te}$ sample, in addition to the softening mentioned above, a narrowing of the B_{1g} phonon is observed, in agreement with recent report on $\text{Fe}_{1.05}\text{Te}$.³⁹

The temperature dependence of both frequency and FWHM of the B_{1g} phonon of the $\text{Fe}_{0.99}\text{Te}_{0.69}\text{Se}_{0.31}$, $\text{Fe}_{0.98}\text{Te}_{0.66}\text{Se}_{0.34}$ and $\text{Fe}_{0.95}\text{Te}_{0.56}\text{Se}_{0.44}$ samples can be well fitted assuming a symmetric anharmonic decay of this optical phonon, *i.e.* decay into two acoustic modes with identical frequencies and opposite momenta,^{45,46}

$$\omega_{ph}(T) = \omega_0 - C \left[1 + \frac{2}{e^{\frac{\hbar\omega_0}{2k_B T}} - 1} \right] \quad (1)$$

$$\Gamma_{ph}(T) = \Gamma_0 + \Gamma \left[1 + \frac{2}{e^{\frac{\hbar\omega_0}{2k_B T}} - 1} \right] \quad (2)$$

where C and Γ are positive constants, ω_0 is the bare phonon frequency, and Γ_0 a residual (temperature-independent) linewidth originating from sample imperfections or electron-phonon interactions. The fitting parameters for these three samples are summarized in Table II. For the $\text{Fe}_{1.02}\text{Te}$ and $\text{Fe}_{1.00}\text{Te}_{0.78}\text{Se}_{0.22}$ samples, as the FWHM increases with decreasing temperature, we can simply not use the latter expression to fit the experimental data.

B. Effect of the iron excess

1. Undoped compounds

Before discussing the possible origin of this unusual evolution of the temperature dependence of the B_{1g} mode FWHM, it is interesting to discuss its dependence with the concentration of Fe excess. We show in Fig. 5-a the raw Raman data obtained at room temperature on the two Se-free samples $\text{Fe}_{1.02}\text{Te}$ and $\text{Fe}_{1.09}\text{Te}$ where the excess iron concentration has been measured to be 2%, and 9%. No strong differences can be found at first glance. The strong aging effect reported in ref.³⁷ has also been observed in our Fe_{1+y}Te samples, as seen in Fig. 5-b, as well as on the Se-substituted samples (not shown here). The origin of this strong Raman signal is not clear. In ref.³⁷, the authors attribute it to the formation of amorphous Te as a decomposition product of $\text{Fe}_{1+y}\text{Te}_{1-x}\text{Se}_x$ on the basis of earlier reports^{47,48}. In particular, in Fig. 2-d from ref.⁴⁷, the authors say that the room temperature spectra of amorphous Te is plotted, but in a note added in proof, they recognize that it rather originates from tetragonal TeO_2 (the Raman spectra of single crystalline paratellurite TeO_2 reported in ref.⁴⁸ shows a much complex structure). We have added these data to our Fig. 5-a and found them not inconsistent with the measurements from our aged surface. The main differences are the relative intensities and widths of the two features of TeO_2 at 120 and 145 cm^{-1} that may originate either from different texturing and strain of TeO_2 and/or from the presence of Fe in the decomposition product.

The excess iron induces a small softening of the A_{1g} mode (Fig. 6-a) but does not affect its already broad linewidth (Fig. 6-c). No changes in the temperature dependence are seen. Similarly, the case of the B_{1g} mode appears to be more interesting. In the excess-Fe rich sample $\text{Fe}_{1.09}\text{Te}$, a small softening through the magnetic transition can still be observed (Fig. 6-b), but the signature of this transition in the FWHM is clearly suppressed (Fig. 6-d). We note finally that the unusual broadening of the mode with decreasing temperature in the parent compounds is observed irrespective to the measured excess iron concentration (fig. 6-d), ruling out a disorder origin for this phenomena.

2. Se-substituted compounds

We now discuss the effect of the excess iron on the vibrational properties for the Se-rich compounds. As seen directly by comparing the data in Figs. 2-b and -c, the low temperature behavior of the phonons is strongly affected by the Fe concentration. In the case of $\text{Fe}_{0.95}\text{Te}_{0.56}\text{Se}_{0.44}$, as already discussed, regular hardening and narrowing of the phonon are observed as temperature is lowered. This is true between room temperature and 60 K for the $\text{Fe}_{1.05}\text{Te}_{0.58}\text{Se}_{0.42}$ sample, with a very close Se content to those of $\text{Fe}_{0.95}\text{Te}_{0.56}\text{Se}_{0.44}$ but where $\sim 5\%$ of excess Fe

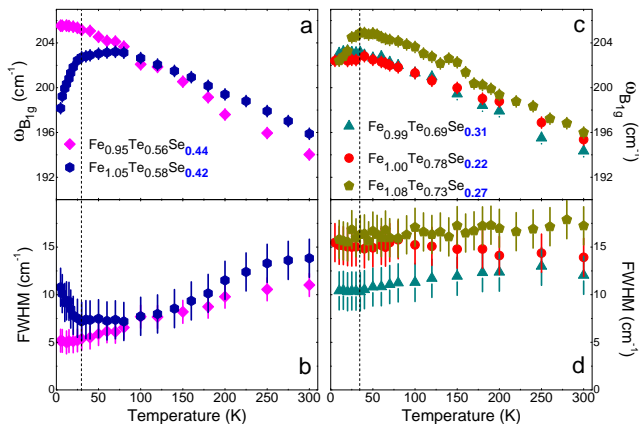


FIG. 7: (Color online) a) and c) Effect of the Fe excess on the temperature dependence of the B_{1g} mode frequency in Se-substituted samples. b) and d) Effect of the Fe excess on the temperature dependence of the B_{1g} mode linewidth in Se-substituted samples.

has been measured. A sudden upturn in this behavior is observed for lower temperature, since at 5K the mode is softer and broader than at 60K. This can be better seen on Figs 7-a and b, where we compare the temperature dependence of frequencies and linewidth of the B_{1g} mode for these two samples. Clearly, as temperature decreases, the phonon hardens and narrows regularly, just as in absence of excess iron, but at a temperature of about 35 K the mode starts to broaden ($\sim 3 \text{ cm}^{-1}$) and softens ($\sim 5 \text{ cm}^{-1}$). In samples with lower Se contents a similar, although weaker, softening of the phonon is observed in the same temperature range, but with no change in the linewidth. None of these effects were observed on the A_{1g} phonon (not shown here).

C. Summary of the experimental results

To summarize our main experimental findings, we observe the following:

- i) For null or low Se concentration, an unusual broadening of the B_{1g} phonon FWHM as temperature is decreased. This progressively turns into a conventional anharmonic narrowing as Se is substituted to Te.
- ii) Clear softening and narrowing of this B_{1g} phonon through the magnetic transition in the parent compound, suppressed in presence of Fe excess.
- iii) Strong softening and broadening of the B_{1g} mode at low temperature in Se substituted samples.

IV. LDA DFT CALCULATIONS

In order to gain further insights on the effects of magnetism and Fe concentration on the lattice dynamics in these systems, we have performed DFT calculations of the frequency of the A_{1g} and B_{1g} modes in both paramagnetic (non-spin-polarized, nsp hereafter) and double stripe ordered (spin-polarized, sp) phases. We start with the results obtained for stoichiometric FeTe system using the frozen phonon approach, summarized in Table III.⁴⁹ Consistently with previous calculations,^{50,51} we find a value of the double-stripe magnetic moment at $y = 0$ ($m = 2.2\mu_B$), which is close to the experimental one.

TABLE III: A_{1g} and B_{1g} frequencies of FeTe, from non-spin-polarized (ω_{nsp}) and spin-polarized (ω_{sp}) DFT calculations.

mode	ω_{nsp} (cm^{-1})	ω_{sp} (cm^{-1})	exp. at 10 K (cm^{-1}) Fe _{1.02} Te sample
A_{1g}	135	175	159.7
B_{1g}	200.9	197.5	200.5

We then consider the effect of Fe excess and deficiencies on the B_{1g} mode. Non-stoichiometry was considered within the VCA, which amounts to replacing Fe with a “virtual” atom with charge $Z_{Fe}^{\pm y}$ in the self-consistent DFT calculations. This means that the average potential due to doping is treated self-consistently, but the effects of randomness are disregarded. Since, within VCA, it is impossible to model the isovalent Se/Te substitution, we do not address the issue of the dependence of the A_{1g} mode on Se/Te concentration in this work. A proper description would require large supercell calculations, beyond the scope of the present paper. We used the FeTe experimental lattice parameters and Te height for all Fe concentrations.²² For each value of the Fe excess y , the frequencies were calculated for nsp and sp configurations.⁴⁹ The frequencies we obtained are given in Table IV, together with the self-consistent value of the magnetic moment at equilibrium.

The values of the calculated frequencies are extremely sensitive to the Fe excess content, which also affects strongly the magnetic moment. In the VCA, the mag-

TABLE IV: B_{1g} frequencies of Fe_{1+y}Te, from non-spin-polarized (ω_{nsp}) and spin-polarized (ω_{sp}) DFT calculations. m is the value of the self-consistent double-stripe moment at zero displacement, in μ_B .

	ω_{nsp} (cm^{-1})	ω_{sp} (cm^{-1})	m (μ_B)
Fe _{0.98} Te	216.76	207.36	2.34
Fe _{0.99} Te	207.21	199.92	2.28
FeTe	200.94	197.54	2.20
Fe _{1.02} Te	191.30	192.40	2.06
Fe _{1.06} Te	173.00	182.00	1.60

netic moments and frequencies decrease monotonically with increasing Fe content, up to the highest doping we calculated ($y = 0.06$). We find an almost linear increase of the B_{1g} frequency with doping, with a linear slope of 523 and 292 cm^{-1}/y for nsp and sp calculations, respectively. As discussed in the next section, the experimentally observed effects of Fe non stoichiometry are much weaker.

V. DISCUSSION

A. Phonon Renormalization through T_N : comparison with other families

In parent $\text{Fe}_{1.02}\text{Te}$, we have observed a clear softening and a narrowing of the B_{1g} phonon through the magnetic ordering transition at T_N . Such narrowing has also been reported in parent BaFe_2As_2 ^{25,26} and CaFe_2As_2 ³² through the spin-density wave (SDW) transition. In the latter case only, it is accompanied by a jump of the phonon frequency that can, at least partially, be explained by the sudden collapse of the unit cell along the c -axis through the transition (such collapse does not take place in BaFe_2As_2).

On the contrary, in Fe_{1+y}Te , the c -axis lattice parameter has been found to expand slightly through the coupled structural-magnetic transition.²⁰ This certainly favors the observed softening, although one would in this case expect an abrupt jump in the phonon frequency at T_N (the structural transition is first-order) rather than the observed smooth softening between T_N and 10 K.

Regarding the agreement with the calculated phonon frequencies, it has been shown for the 122 and 1111 systems that the experimental phonon frequencies are closer from those obtained with a magnetic calculation than from those where magnetism is not included, even in the paramagnetic state.^{24,33,34,52} This is also the case here as we get a better match with our experimental data using the sp calculation rather than the nsp one (see Sect. IV).

Finally, as the phonon linewidth is inversely proportional to the lifetime of the excitation, its renormalization through T_N reflects the changes in the coupling of the phonons to some decay channels. In the 122 arsenides, as the SDW gap opens,^{53,54} a significant reduction of the electronic density of states at the Fermi level occurs, leading to a decrease of electron-phonon coupling that reasonably accounts for the observed sharpening of the phonons.²⁵ Such an SDW gap opening has not yet been reported in the 11 compounds,^{55,56} but has recently been observed in ARPES experiments⁵⁷ and is very likely responsible for the B_{1g} mode narrowing in the $\text{Fe}_{1.02}\text{Te}$ sample.

B. Se-substituted systems

1. Absence of superconductivity induced anomalies

As mentioned in the Introduction, the B_{1g} Fe mode that shows here the most striking doping dependence is active in all the families of Fe-based superconductors. The absence of renormalization of this phonon as well as of the A_{1g} one through the superconducting transition in the doped compounds is consistent with experiments carried out on the doped 122 arsenide compounds²⁵ (with the notable exception being the electron-doped $\text{Pr}_x\text{Ca}_{1-x}\text{Fe}_2\text{As}_2$,³⁶ where a small hardening of the B_{1g} phonon through T_c has been observed) or on the 111 compound LiFeAs ³⁵, where no signature of the superconducting transition is seen either in the frequency or in the linewidth of these two modes. This is due to the fact that the superconducting gap amplitude is smaller than the phonon frequencies, hence their opening let them unaffected. The situation is similar for the 11 compounds, as the phonon frequency is much larger than the energies reported for the superconducting gap(s) in various experiments [$2\Delta \sim 2$ meV (17 cm^{-1})⁵⁸, 3.4 meV (27.4 cm^{-1})⁵⁹ or 4.6 meV (37 cm^{-1})⁶⁰ from STM, $2\Delta \sim 3$ meV (24 cm^{-1}) from NMR,⁶¹ and $2\Delta \sim 6$ meV (48 cm^{-1}) from specific heat⁴²].

2. Se-substitution induced evolution of the B_{1g} mode FWHM temperature dependence

We now turn to the influence of Se concentration on the behavior of the B_{1g} phonon. As it is substituted into the system, we observe a weak increase of the B_{1g} phonon frequency at the lowest temperatures (see Figs. 4 b to e), that goes along with the reduction of the c -axis parameter reported from x-ray and neutron diffraction experiments.^{7,10,20} The room temperature linewidth for this mode is only weakly dependent on the Se concentration, although the FWHM clearly tends to sharpen with increasing Se content. This fact is already surprising as one may have rather expected the Se-substitution induced disorder to favor a broadening of the phonon line-shape instead of a narrowing. The normal state temperature dependence of the mode FWHM for different doping levels is even more puzzling. As noted in Sec. III A, the situation appears conventional in the $\text{Fe}_{0.95}\text{Te}_{0.56}\text{Se}_{0.44}$ samples close to half doping, with a continuous narrowing of the phonon with decreasing temperature. On the contrary, as Se contents are reduced the phonon broadens with decreasing temperature. This is particularly clear for the two Se-free samples ($\text{Fe}_{1.02}\text{Te}$ and $\text{Fe}_{1.09}\text{Te}$), as seen in Fig. 6-d.

The temperature dependence of the three samples with the highest Se content have successfully been fitted using a conventional anharmonic decay model (Eq. 2). Interestingly, looking at the fitting parameters of Table II, the residual - or temperature-independent - linewidth Γ_0 (3.4

cm^{-1}) in $\text{Fe}_{0.95}\text{Te}_{0.56}\text{Se}_{0.44}$ is comparable with the one of the temperature dependent parameter Γ (2.1 cm^{-1}), whereas in $\text{Fe}_{0.98}\text{Te}_{0.66}\text{Se}_{0.34}$ and $\text{Fe}_{0.99}\text{Te}_{0.69}\text{Se}_{0.31}$ we have $\Gamma_0 \sim 10 \text{ cm}^{-1} \gg \Gamma$.

The situation is thus much closer to the one reported for $\text{Pr}_x\text{Ca}_{1-x}\text{Fe}_2\text{As}_2$ ³⁶ than for LiFeAs , where the residual linewidth was always vanishingly small.³⁵ This shows that in $\text{Fe}_{1+y}\text{Te}_{1-x}\text{Se}_x$ systems, the contribution of anharmonicity to the B_{1g} phonon lifetime is not the dominant one. An additional decay channel for this phonon must therefore take over the usual anharmonic effects, and its contribution increases strongly as Se content is decreased. Such behavior can have at least two possible origins: electron-phonon coupling and spin-phonon coupling. In the first scenario, the increasing relative weight Γ_0 with decreasing Se content can be trivially related to the increase of the electronic density of states at the Fermi level $N(E_F)$ ⁵⁰ [as $\Gamma_0 \propto N(E_F)$]. This may, however, not be sufficient to account for the reported effect: Electron-phonon coupling is, in principle, temperature independent and can, therefore, hardly explain the increasing linewidth of the B_{1g} phonon with decreasing temperature in the systems with the lowest Se contents ($\text{Fe}_{1.02}\text{Te}$, $\text{Fe}_{1.00}\text{Te}_{0.78}\text{Se}_{0.22}$). Having in mind the increasing weight of magnetic excitations as Se concentration decreases toward the parent compound,¹⁸ we are naturally led to suggest that spin-phonon coupling may be the additional decay channel for the phonons. The effects of excess Fe discussed in the next section indeed confirm an interplay between the lattice and spin degrees of freedom in these systems.

C. Influence of the iron concentration

1. Comparison of experimental data with LDA DFT calculation

According to our calculation in Sec. IV, increasing the Fe concentration induces a softening of the B_{1g} mode frequencies in both sp and nsp calculations. The softening rates are found to be 523 and $292 \text{ cm}^{-1}/y$ for nsp and sp, respectively. Experimentally, at low temperature, a small hardening is instead observed in the parent compounds, when going from $\text{Fe}_{1.02}\text{Te}$ to $\text{Fe}_{1.09}\text{Te}$. In Se-substituted samples on the other hand, a $\sim 7 \text{ cm}^{-1}$ softening between $\text{Fe}_{0.95}\text{Te}_{0.56}\text{Se}_{0.44}$ and $\text{Fe}_{1.05}\text{Te}_{0.58}\text{Se}_{0.42}$ B_{1g} phonon frequencies is indeed observed ($\sim 70 \text{ cm}^{-1}/y$). An effect of comparable size is found when comparing the B_{1g} peak frequencies of $\text{Fe}_{0.95}\text{Te}_{0.56}\text{Se}_{0.44}$ ($\omega_{B_{1g}} = 205.6 \text{ cm}^{-1}$) and $\text{Fe}_{0.98}\text{Te}_{0.66}\text{Se}_{0.34}$ ($\omega_{B_{1g}} = 203.8 \text{ cm}^{-1}$), with significantly different Fe deficiencies (even though the Se concentrations in this case slightly differ). This gives a softening rate of $\sim 66 \text{ cm}^{-1}/y$.

In any case, the experimentally observed effects of Fe nonstoichiometry are much weaker than those theoretically calculated, even considering the sp calculation where they are the smallest. One has to keep in mind

that accurate comparison to the calculation is tough as the presence of excess ($y > 0$) Fe complicates the situation. In fact, in the VCA there is no qualitative difference between Fe excess and deficiency, as the excess (deficient) charge are both located around the Fe site. Experimentally, however, it is known that the excess Fe ions are located in the Te planes, and this has qualitatively different effects, the most important being that the effective Fe magnetic moment is enhanced and not reduced, due to the formation of local moments on the excess Fe in the Te planes. This cannot be taken into account by the VCA approach of treating the doping in our LDA calculations. Furthermore, it is important to point out that mean-field LDA DFT calculations cannot reproduce the renormalization of the B_{1g} frequency and linewidth observed at low temperature in the Fe-rich systems, which are discussed in the next paragraph.

2. Excess Fe-induced magnetic fluctuation

We have seen in Sec. IIIB1 that in the $\text{Fe}_{1.09}\text{Te}$ crystal, we are not able to observe clearly the effect of the magnetic transition on the phonons. A small softening has been seen (see Fig. 6-d), but no narrowing of the line shape. In the Se-substituted system, as shown in Fig. 7, excess iron, in addition to a decrease in T_c , induces large effects on both frequency and lineshape of the phonons. The strongest effect occurs close to 50% Se content, with a large softening and broadening of the B_{1g} phonon below $T \sim 35 \text{ K}$, well above T_c . To our knowledge, no phase transition has been reported in this temperature range for this doping level, but the occurrence of short-range magnetic fluctuations has been reported.¹⁶ In the undoped case with low excess iron concentration, it has been shown that a low energy gap in the spin-wave excitation spectrum opens when entering the magnetic state.⁴⁰ Increasing the excess iron concentration, this gap is filled up with low-energy spin fluctuations.⁴⁰

In both doped and undoped cases, one effect of excess iron is, therefore, to induce low energy magnetic fluctuations in a temperature range at which we also observe a relative broadening of the B_{1g} phonon, *i. e.*, a decrease of its lifetime. This reinforces the point we made at the end of Sec. VB2, indicating that the additional damping for the B_{1g} mode may actually originate from its coupling to magnetic excitations.

VI. CONCLUSIONS

We have carried out a systematic study of the lattice dynamics in the $\text{Fe}_{1+y}\text{Te}_{1-x}\text{Se}_x$ system, focusing more particularly on the c -axis polarized Fe B_{1g} mode. In parent compounds, unlike other systems such as BaFe_2As_2 or LiFeAs , a nonconventional broadening of this mode is observed as temperature decreases, and a clear signature of the SDW gap opening is observed. As Se is substi-

tuted to Te, the temperature dependence of this modes smoothly evolves toward a more regular situation, with the B_{1g} phonon showing conventional anharmonic decay. A good agreement between the observed phonon frequencies and a first-principles calculation including the effects of magnetic ordering is found. The temperature dependence of the phonon linewidth, as well as the effects induced by the Fe nonstoichiometry in these compounds, revealed a peculiar coupling of this mode to magnetic fluctuations in the $\text{Fe}_{1+y}\text{Te}_{1-x}\text{Se}_x$ system and can, to date, not be satisfactorily reproduced within state-of-the-art computational approaches.

VII. ACKNOWLEDGEMENT

We thank A. Schulz for technical support and A.C. Walters for useful suggestions. This work has been supported by the European project SOPRANO (Grant No. PITN-GA-2008-214040), by the French National Research Agency, (Grant No. ANR-09-Blanc-0211 SupraTetrafer), and by the UK Engineering and Physical Sciences Research Council (MJR, EP/C511794).

-
- ¹ Y. Kamihara, T. Watanabe, M. Hirano, H. Hosono, *J. Am. Chem. Soc.* **130**, 3296 (2008).
 - ² H. Takahashi, K. Igawa, K. Arii, Y. Kamihara, M. Hirano, and H. Hosono, *Nature (London)* **453**, 376 (2008).
 - ³ Z.-A. Ren, W. Lu, J. Yang, W. Yi, X.-L. Shen, C. Zheng, G.-C. Che, X.-L. Dong, L.-L. Sun, F. Zhou, and Z.-X. Zhao, *Chinese Physics Letters* **25**, 2215 (2008).
 - ⁴ M. Rotter, M. Tegel, and D. Johrendt, *Phys. Rev. Lett.* **101**, 107006 (2008).
 - ⁵ J. H. Tapp, Z. Tang, B. Lv, K. Sasmal, B. Lorenz, P. C. W. Chu, and A. M. Guloy, *Phys. Rev. B* **78**, 060505 (2008).
 - ⁶ F. C. Hsu, J. Y. Luo, K. W. Yeh, T. K. Chen, T. W. Huang, P. M. Wu, Y. C. Lee, Y. L. Huang, Y. Y. Chu, D. C. Yan, and M. K. Wu, *Proc. Natl. Acad. Sci. USA*, **105**, 14262 (2008).
 - ⁷ K. W. Yeh, T. W. Huang, Y. L. Huang, T. K. Chen, F. C. Hsu, P. M. Wu, Y. C. Lee, Y. Y. Chu, C. L. Chen, J. Y. Luo, D. C. Yan, and M. K. Wu, *Europhys. Lett.* **84**, 37002 (2008).
 - ⁸ M. H. Fang, H. M. Pham, B. Qian, T. J. Liu, E. K. Vehstedt, Y. Liu, L. Spinu, and Z. Q. Mao, *Phys. Rev. B* **78**, 224503 (2008).
 - ⁹ D. Fruchart, P. Convert, P. Wolfers, R. Madar, J. P. Seneater, and R. Fruchart, *Mater. Res. Bull.* **10**, 169 (1975).
 - ¹⁰ S. Li, C. de la Cruz, Q. Huang, Y. Chen, J. W. Lynn, J. Hu, Y. L. Huang, F. C. Hsu, K. W. Yeh, M. K. Wu, and P. C. Dai, *Phys. Rev. B* **79**, 054503 (2009).
 - ¹¹ F. Ma, W. Ji, J. Hu, Z. Y. Lu, and T. Xiang, *Phys. Rev. Lett.* **102**, 177003 (2009).
 - ¹² M. J. Han and S. Y. Savrasov, *Phys. Rev. Lett.* **103**, 067001 (2009).
 - ¹³ W. Bao, Y. Qiu, Q. Huang, M.A. Green, P. Zajdel, M.R. Fitzsimmons, M. Zhernenkov, S. Chang, M. Fang, B. Qian, E.K. Vehstedt, J. Yang, H.M. Pham, L. Spinu, Z.Q. Mao, *Phys. Rev. Lett.* **102**, 247001 (2009).
 - ¹⁴ C. de la Cruz, Q. Huang, J. W. Lynn, J. Li, W. R. Li, J. L. Zarestky, H. A. Mook, G. F. Chen, J. L. Luo, N. L. Wang, and P. Dai, *Nature*, **453**, 899 (2008).
 - ¹⁵ D.J. Singh, and M.H. Du, *Phys. Rev. Lett.* **100**, 237003 (2008).
 - ¹⁶ R. Khasanov, M. Bendele, A. Amato, P. Babkevich, A. T. Boothroyd, A. Cervellino, K. Conder, S.N. Gvasaliya, H. Keller, H.-H. Klauss, H. Luetkens, V. Pomjakushin, E. Pomjakushina, and B. Roessli, *Phys. Rev. B* **80**, 140511(R) (2009).
 - ¹⁷ L. Zhang, D. J. Singh, and M. H. Du, *Phys. Rev. B* **79**, 012506 (2009).
 - ¹⁸ J. Wen, G. Xu, Z. Xu, Z. W. Lin, Q. Li, W. Ratcliff, G. Gu, and J. M. Tranquada, *Phys. Rev. B* **80**, 104506 (2009).
 - ¹⁹ T. J. Liu, X. Ke, B. Qian, J. Hu, D. Fobes, E. K. Vehstedt, H. Pham, J. H. Yang, M. H. Fang, L. Spinu, P. Schiffer, Y. Liu, and Z. Q. Mao, *Phys. Rev. B* **80**, 174509 (2009).
 - ²⁰ A. Martinelli, A. Palenzona, M. Tropeano, C. Ferdeghini, M. Putti, M. R. Cimberle, T. D. Nguyen, M. Affronte, and C. Ritter, *Phys. Rev. B* **81**, 094115 (2010).
 - ²¹ Z. Xu, J. Wen, G. Xu, S. Chi, W. Ku, G. Gu, and J. M. Tranquada, *Phys. Rev. B* **84**, 052506 (2011).
 - ²² M. Bendele, P. Babkevich, S. Katrych, S. N. Gvasaliya, E. Pomjakushina, K. Conder, B. Roessli, A. T. Boothroyd, R. Khasanov, and H. Keller, *Phys. Rev. B* **82**, 212504 (2010).
 - ²³ A. P. Litvinchuk, V. G. Hadjiev, M. N. Iliev, B. Lv, A. M. Guloy, and C. W. Chu, *Phys. Rev. B* **78**, 060503(R) (2008).
 - ²⁴ D. Reznik, K. Lokshin, D. C. Mitchell, D. Parshall, W. Dmowski, D. Lamago, R. Heid, K. P. Bohnen, A. S. Sefat, M. A. McGuire, B. C. Sales, D. G. Mandrus, A. Subedi, D. J. Singh, A. Alatas, M. H. Upton, A. H. Said, A. Cunsolo, Y. Shvydko, and T. Egami, *Phys. Rev. B* **80**, 214534 (2009).
 - ²⁵ M. Rahlenbeck, G. L. Sun, D. L. Sun, C. T. Lin, B. Keimer, and C. Ulrich, *Phys. Rev. B* **80**, 064509 (2009).
 - ²⁶ L. Chauvière, Y. Gallais, M. Cazayous, A. Sacuto, M. A. Measson, D. Colson, and A. Forget, *Phys. Rev. B* **80**, 094504 (2009).
 - ²⁷ Y. Gallais, A. Sacuto, M. Cazayous, P. Cheng, L. Fang, and H. H. Wen, *Phys. Rev. B* **78**, 132509 (2008).
 - ²⁸ K. Y. Choi, D. Wulferding, P. Lemmens, N. Ni, S. L. Budko, and P. C. Canfield, *Phys. Rev. B* **78**, 212503 (2008).
 - ²⁹ M. Le Tacon, M. Krisch, A. Bosak, J. W. G. Bos, and S. Margadonna, *Phys. Rev. B* **78**, 140505 (2008).
 - ³⁰ T. Fukuda, A. Q. R. Baron, S.-i. Shamoto, M. Ishikado, H. Nakamura, M. Machida, H. Uchiyama, S. Tsutsui, A. Iyo, H. Kito, J. Mizuki, M. Arai, H. Eisaki, and H. Hosono, *Journ. Phys. Soc. Jap.*, **77**, 103715 (2008).
 - ³¹ M. Le Tacon, T. R. Forrest, Ch. Rüegg, A. Bosak, A. C. Walters, R. Mittal, H. M. Rønnow, N. D. Zhigadlo, S. Katrych, J. Karpinski, J. P. Hill, M. Krisch, and D. F. McMorrow, *Phys. Rev. B* **80**, 220504(R) (2009).
 - ³² K.-Y. Choi, P. Lemmens, I. Eremin, G. Zwirgagl, H. Berger, G. L. Sun, D. L. Sun, and C. T. Lin, *J. Phys.: Condens. Matter* **22**, 115802 (2010).

- ³³ S. E. Hahn, Y. Lee, N. Ni, P. C. Canfield, A. I. Goldman, R. J. McQueeney, B. N. Harmon, A. Alatas, B. M. Leu, E. E. Alp, D. Y. Chung, I. S. Todorov, and M. G. Kanatzidis, *Phys. Rev. B* **79**, 220511 (2009).
- ³⁴ T. Fukuda, A. Q. R. Baron, H. Nakamura, S. Shamoto, M. Ishikado, M. Machida, H. Uchiyama, A. Iyo, H. Kito, J. Mizuki, M. Arai, and H. Eisaki, *Phys. Rev. B* **84**, 064504 (2011).
- ³⁵ Y. J. Um, J. T. Park, B. H. Min, Y. J. Song, Y. S. Kwon, B. Keimer, and M. Le Tacon, *Phys. Rev. B* **85**, 012501 (2012).
- ³⁶ A. P. Litvinchuk, B. Lv, and C. W. Chu, *Phys. Rev. B* **84**, 092504 (2011).
- ³⁷ T.-L. Xia, D. Hou, S. C. Zhao, A. M. Zhang, G. F. Chen, J. L. Luo, N. L. Wang, J. H. Wei, Z.-Y. Lu, and Q. M. Zhang, *Phys. Rev. B* **79**, 140510(R) (2009).
- ³⁸ K. Okazaki, S. Sugai, S. Niitaka, and H. Takagi, *Phys. Rev. B* **83**, 035103 (2011).
- ³⁹ V. Gnezdilov, Y. Pashkevich, P. Lemmens, A. Gusev, K. Lamonova, T. Shevtsova, I. Vitebskiy, O. Afanasiev, S. Gnatchenko, V. Tsurkan, J. Deisenhofer, and A. Loidl, *Phys. Rev. B* **83**, 245127 (2011).
- ⁴⁰ C. Stock, E. E. Rodriguez, M. A. Green, P. Zavalij, and J. A. Rodriguez-Rivera, *Phys. Rev. B* **84**, 045124 (2011).
- ⁴¹ Y. Liu and C.T. Lin, *Journal of Superconductivity and Novel Magnetism* **84**, 183 (2011).
- ⁴² T. Klein, D. Braithwaite, A. Demuer, W. Knafo, G. Laperot, C. Marcenat, P. Rodière, I. Sheikin, P. Strobel, A. Sulpice, and P. Toulemonde, *Phys. Rev. B* **82**, 184506 (2010).
- ⁴³ A. Tamai, A. Y. Ganin, E. Rozbicki, J. Bacsá, W. Meevasana, P. D. C. King, M. Caffio, R. Schaub, S. Margadonna, K. Prassides, M. J. Rosseinsky, and F. Baumberger, *Phys. Rev. Lett.* **104**, 097002 (2010).
- ⁴⁴ N. C. Gresty, Y. Takabayashi, A. Y. Ganin, M. T. McDonald, J. B. Claridge, D. Giap, Y. Mizuguchi, Y. Takano, T. Kagayama, Y. Ohishi, M. Takata, M. J. Rosseinsky, S. Margadonna, and K. Prassides, *Journal of the American Chemical Society*, **131**, 16944 (2009).
- ⁴⁵ P. G. Klemens, *Phys. Rev.* **148**, 845 (1966).
- ⁴⁶ J. Menéndez, and M. Cardona, *Phys. Rev. B* **29**, 2051 (1984).
- ⁴⁷ A. S. Pine, and G. Dresselhaus, *Phys. Rev. B* **4**, 356 (1971).
- ⁴⁸ A. S. Pine, and G. Dresselhaus, *Phys. Rev. B* **5**, 4087 (1972).
- ⁴⁹ We used the LDA approximation for the exchange correlation functional, and the linearly-augmented plane wave (LAPW) basis set with local orbitals. The \mathbf{k} -point integration was performed on a 4 8 4 grid for the doubled unit cell. The experimental lattice parameters are $a=3.826\text{\AA}$ and $c=6.273\text{\AA}$, with $z_{Te}=0.28141$.
- ⁵⁰ A. Subedi, L. Zhang, D. J. Singh, and M. H. Du, *Phys. Rev. B* **78**, 134514 (2008).
- ⁵¹ Lijun Zhang, D. J. Singh, and M. H. Du, *Phys. Rev. B* **79**, 012506 (2009).
- ⁵² L. Boeri, M. Calandra, I. I. Mazin, O. V. Dolgov, and F. Mauri, *Phys. Rev. B* **82**, 020506 (2010).
- ⁵³ A. Akrap, J. J. Tu, L. J. Li, G. H. Cao, Z. A. Xu, and C. C. Homes, *Phys. Rev. B* **80**, 180502 (2009).
- ⁵⁴ A. V. Boris, N. N. Kovaleva, S. S. A. Seo, J. S. Kim, P. Popovich, Y. Matiks, R. K. Kremer, and B. Keimer, *Phys. Rev. Lett.* **102**, 027001 (2009).
- ⁵⁵ G. F. Chen, Z. G. Chen, J. Dong, W. Z. Hu, G. Li, X. D. Zhang, P. Zheng, J. L. Luo, and N. L. Wang, *Phys. Rev. B* **79**, 140509 (2009).
- ⁵⁶ Y. Xia, D. Qian, L. Wray, D. Hsieh, G. F. Chen, J. L. Luo, N. L. Wang, and M. Z. Hasan, *Phys. Rev. Lett.* **103**, 037002 (2009).
- ⁵⁷ M. Månsson, private communication.
- ⁵⁸ Y. Noat, T. Cren, V. Dubost, S. Lange, F. Debontridder, P. Toulemonde, J. Marcus, A. Sulpice, W. Sacks, and D. Roditchev, *J. Phys. Condens. Mat.* **22**, (2010).
- ⁵⁹ T. Hanaguri, S. Niitaka, K. Kuroki, and H. Takagi, *Science* **328**, 474 (2010).
- ⁶⁰ T. Kato, Y. Mizuguchi, H. Nakamura, T. Machida, H. Sakata, and Y. Takano, *Phys. Rev. B* **80**, 180507 (2009).
- ⁶¹ D. Arčon, P. Jeglič, A. Zorko, A. Potočnik, A. Y. Ganin, Y. Takabayashi, M. J. Rosseinsky, and K. Prassides, *Phys. Rev. B* **82**, 140508 (2010).